The Astrophysical Journal, 605:546–553, 2004 April 10

MAGNETIC FIELD, Hα, AND *RHESSI* OBSERVATIONS OF THE 2002 JULY 23 GAMMA-RAY FLARE

Vasyl Yurchyshyn
Big Bear Solar Observatory, Big Bear City, CA 92314

Haimin Wang
Big Bear Solar Observatory, Big Bear City, CA 92314

Valentyna Abramenko
Big Bear Solar Observatory, Big Bear City, CA 92314; and Crimean Astrophysical Observatory, 98409 Nauchny, Ukraine

Thomas J. Spirock
Big Bear Solar Observatory, Big Bear City, CA 92314

and

Säm Krucker
Space Sciences Laboratory, University of California, Berkeley, CA 94720
Received 2003 May 9; accepted 2003 December 18

ABSTRACT

In this paper we examine two aspects of the 2002 July 23 gamma-ray flare by using multiwavelength observations. First, the data suggest that the interaction of the erupted field with an overlying large-scale coronal field can explain the offset between the gamma-ray and the hard X-ray sources observed in this event. Second, we pay attention to rapid and permanent changes in the photospheric magnetic field associated with the flare. MDI and BBSO magnetograms show that the following magnetic flux had rapidly decreased by 1×10^{20} Mx immediately after the flare, while the leading polarity was gradually increasing for several hours after the flare. Our study also suggests that the changes were most probably associated with the emergence of new flux and the reorientation of the magnetic field lines. We interpret the magnetograph and spectral data for this event in terms of the tether-cutting model.

Subject headings: Sun: flares — Sun: magnetic fields

1. INTRODUCTION

Filament eruptions, coronal mass ejections (CMEs), and associated photospheric activity, such as solar flares, indicate an ongoing relaxation of large-scale, highly stressed solar magnetic fields. Release of magnetic energy during such processes is expected to be accompanied by some variations in the magnetic field. Earlier studies report both the localized changes associated with the major polarity inversion line (Severny 1964; Zvereva & Severny 1970; Moore et al. 1984; Kosovichev & Zharkova 1999, 2001; Wang & Tang 1993; Wang et al. 1994, 2002; Cameron & Sammis 1999; Spirock, Yurchyshyn, & Wang 2002) and global changes when the entire photospheric and coronal fields in an active region are involved in a flare (van Driel-Gesztelyi et al. 1997; Aschwanden et al. 1999; Yurchyshyn, Abramenko, & Carbone 2000; Abramenko et al. 2003).

Wang et al. (2002) summarized the results of a study for six X-class flares and found that there were rapid and permanent changes in the magnetic flux related to the impulsive phase of the flares. Moreover, these events exhibited a puzzling signature in that the changes of the magnetic flux of the two polarities were not balanced: the leading flux always increased while the following flux tended to decrease, although by a much smaller amount. Spirock et al. (2002) suggested two possible mechanisms to explain the unbalanced flux variations of the 2002 April 2 flare: (1) the emergence of a very inclined flux tube and/or (2) a change in the orientation of the magnetic field. Later, Wang et al. (2002) offered a third explanation: the expansion of the preceding sunspot, as a result of the relaxation of the magnetic field, after a flare.

Very often, large flares are accompanied by powerful CMEs, which can cause severe geomagnetic storms when expelled toward the Earth. There are several competing approaches to explain magnetic eruptions, and extensive multiwavelength data sets, including magnetic field measurements, can be used to provide a discriminator between different models and/or mechanisms.

One approach has been developed by many authors over the years (van Tend & Kuperus 1978; van Ballegooijen & Martens 1989; Forbes & Isenberg 1991; Kumar & Rust 1996; Wu et al. 1999; Amari et al. 2000). It advocates the idea that the energy for eruptions is stored in a flux rope, which is formed long before the eruption occurs. The tether-cutting model (Moore & LaBonte 1980), on the other hand, suggests that an impulsive major energy release begins deep in a highly sheared core field via reconnection, which forms a flux rope. The released magnetic field then erupts into interplanetary space. All these models predict that no remote EUV and/or Hα emission in quiet-Sun areas outside the site of a flare should precede the eruption.

The breakout model (Antiochos 1998; Antiochos, DeVore, & Klimchuk 1999), instead, assumes that a sheared core field pushes through an overlaying restraining field and that a slow reconnection begins at a neutral point high in the corona. At this stage, EUV crinkles and/or remote Hα brightenings are expected to occur at the footpoints of the overlying field lines involved in the reconnection (Sterling et al. 2001). After the restraining force of the overlying field is significantly weakened because of the reconnection, the sheared core field then explosively erupts into interplanetary space. As the erupted field leaves the lower atmosphere, it stretches the remaining

overlying field lines, which immediately reconnect beneath the escaping magnetic field with releasing magnetic energy and form postflare loops at the site of eruption. There are observations that strongly support this prediction. Sterling & Moore (2001) and Sterling et al. (2001) interpreted the EUV crinkles, which occur before an eruption, as evidence for the breakout model.

We analyze Hα, magnetograph, EUV, and X-ray data for the 2002 July 23 flare observed at the east solar limb. This gamma-ray flare occurred in NOAA Active Region 0039 and was a long-duration event that peaked around 0028 UT. We focus here on the evolution of magnetic fields associated with the flare.

2. OBSERVATIONS

The data set that we used in our study includes vector magnetograms and Hα images from the Big Bear Solar Observatory (BBSO), full-disk longitudinal magnetograms from the Michelson Doppler Imager (MDI), and EUV images from the EUV Imaging Telescope on board the *Solar and Heliosphere Observatory* (*SOHO*) and X-ray data from the *Ramaty High-Energy Solar Spectroscopic Imager* (*RHESSI*).

BBSO's Digital Vector Magnetograph (DVMG) system has a much improved sensitivity and resolution compared with that of the old BBSO Video Magnetograph system. The hardware has been described in detail by Spirock et al. (2001). It consists of a 0.25 Å bandpass filter, an SMD 1024×1024 12 bit CCD camera, and three liquid crystals used as polarization analyzers. Each data set consists of four images taken at the blue wing of the λ6103 spectral line: a filtergram (Stokes I), a line-of-sight magnetogram (Stokes V), and a transverse magnetogram (Stokes U and Q). We usually rebin the camera to the 512×512 pixels to increase the sensitivity of the magnetograms. After rebinning, the pixel resolution is about $0\farcs6$. The line-of-sight magnetic sensitivity is approximately 2 G, while the transverse sensitivity is approximately 20 G. The cadence for a complete set of Stokes images is typically 1 minute.

BBSO magnetograms, used to study this flare, cover two time ranges: (1) from 2000 to 2245 UT on July 22 and (2) from 0037 to 0154 UT on July 23. In order to cover a longer time period and to also have an independent confirmation of BBSO observations, we used 1 minute cadence full-disk MDI magnetograms.

Much of the energy released during a flare is used to accelerate, to very high energies, electrons (emitting primarily X-rays) and protons and other ions (emitting primarily gamma rays). The goal of the *RHESSI* mission is to combine, for the first time, high-resolution imaging in hard X-rays (HXRs) and gamma rays with high-resolution spectroscopy, so that a detailed energy spectrum can be obtained at each point in the image (Lin et al. 2002). *RHESSI* had complete coverage of this flare. In this study we use *RHESSI* data at several energy bands to understand the relationship between the structure of the magnetic field and energy release sites.

3. THE GAMMA-RAY FLARE AS SEEN IN MULTIWAVELENGTH DATA

Figure 1 shows the X4.8 two-ribbon flare on 2002 July 23, which is the sole gamma-ray flare observed by *RHESSI* thus far. The background images are BBSO Hα filtergrams at two different times near the peak of the flare. The corresponding *RHESSI* HXR emission in the 12–20 keV energy band is shown with dashed contours, while the solid contours indicate the HXR emission between 100 and 150 keV. According to Krucker, Hurford, & Lin (2003), the HXR emission, which was dominant above 30 keV, was related to the photospheric footpoints, while the lower energy emission was associated with a gradual coronal X-ray source.

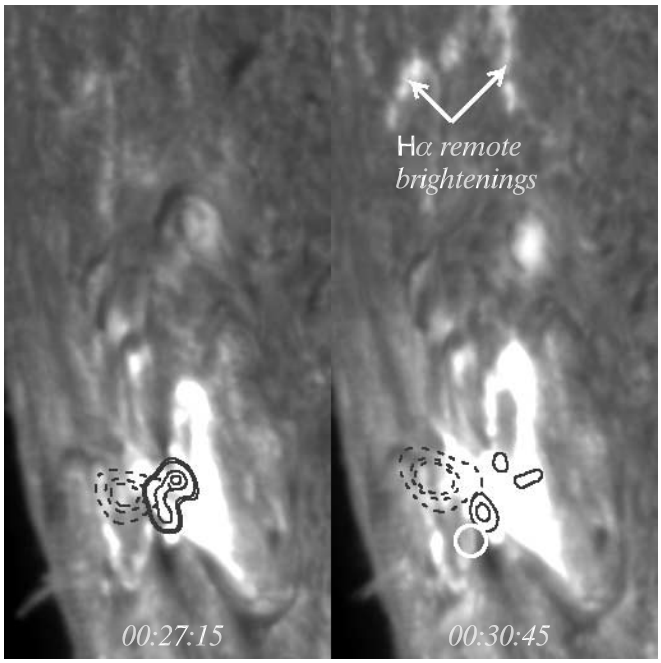

FIG. 1.—BBSO Hα images of the X4.8 two-ribbon flare on 2002 July 23. The field of view is $118'' \times 280''$. The dashed contours are the corresponding *RHESSI* X-ray emissions in the energy range of 12–20 keV, while the solid contours are for the 100–150 keV energy band. The white circle in the right panel shows the position of the 2.223 MeV centroid. North is up, and west is to the right.

In Figure 2 we plot the time history of the Hα, HXR, and gamma-ray emission. The thick line in the top panel of Figure 2 shows Hα flux determined at the flare core, where the HXR sources and flare ribbon were observed. The Hα flare started at 0020 UT, about 7 minutes before the onset of the impulsive HXR emission. The 50–100 keV HXR emission abruptly rises at 002730 UT and peaks at about 002830 UT. Other energy bands (100–300, 800–1900, and 2228–7000 keV) show very similar time profiles. However, the 2218–2228 keV source behaves quite differently. The white circle in Figure 1 shows the position of the 2218–2228 keV emission centroid, which was significantly displaced from the other HXR sources. There is no sudden rise of the 2218–2228 keV emission at the beginning of the flare (Fig. 2, *fourth panel*). Instead, it increases slowly, reaching maximum at about 003138 UT, 4 minutes after the peak in the HXR emission (the gray vertical bar in Fig. 2 shows the FWHM for this gamma-ray source). A weak Hα flare emission and a surge were observed southeast of the gamma-ray centroid.

We would like to emphasize the weak and irregular Hα emission seen at 003045 UT outside the active region (Fig. 1, *arrows*). This remote emission was observed as a chain of Hα brightenings in a remote quiet-Sun area about $160''$ north of the active region (Tang & Moore 1982). The thick line in the fourth panel of Figure 2 shows the average light curve of these remote brightenings. The remote Hα emission began to gradually rise only at the onset of the impulsive HXR flare and reached a maximum at $\sim$003100 UT, about 1 minute earlier

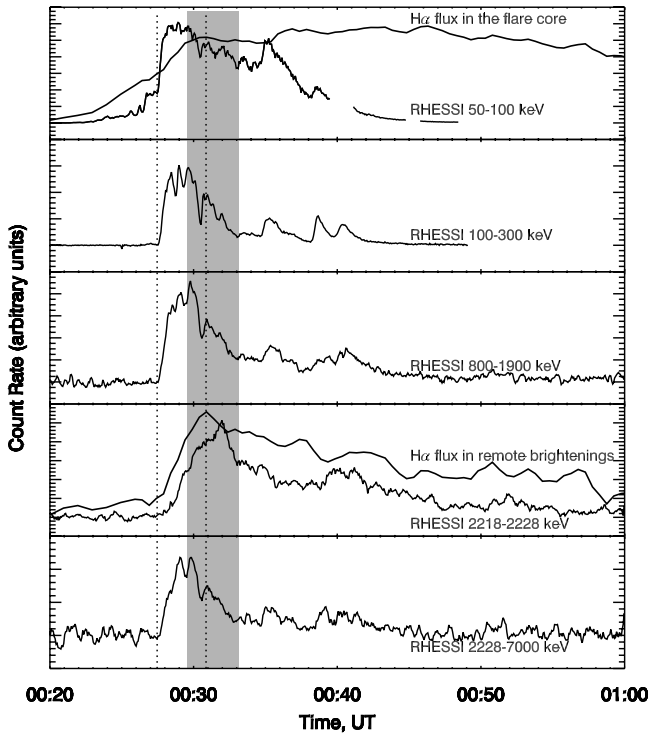

FIG. 2.—*Thin lines*: Light curves for 50–100, 100–300, 800–1900, 2218–2228, and 2228–7000 keV energy bands. *Thick lines*: Hα light curves for the flare core (*top panel*) and for the remote brightenings (*fourth panel*).

than the peak of the 2218–2228 keV source. The comparison between the time profiles for the remote brightenings and those for the gamma-ray source shows that these two light curves are very similar within the 0020–0033 UT time interval. However, the 2218–2228 keV source lags relative to the Hα source by about 60 s. We would also like to note that the peak of the remote Hα brightenings coincides with the well-pronounced secondary peak in the *RHESSI* X-ray flux at 0031 UT (Fig. 2, *right dotted line*).

4. RAPID CHANGES IN THE LONGITUDINAL MAGNETIC FIELD ASSOCIATED WITH THE FLARE

4.1. *Magnetic Flux Changes in the Observed Data*

The MDI data that we have utilized here have longer, more complete coverage and better stability, so we present only the MDI flux time profiles. Figure 3 shows the time profiles of magnetic fluxes and the *RHESSI* HXR flux (arbitrary units) in the 100–150 keV energy range as a function of time. The total MDI fluxes were determined by separately summing positive and negative flux densities inside a box, which enclosed the entire area of the active region shown in Figure 4. The error bars in Figure 3 show the standard deviation determined individually for each magnetogram by calculating the total flux for nine different positions of the box. The flux time profiles are plotted for the leading (negative) and the following (positive) polarity by the thin solid lines. The magnetic field measurements between 0026 and 0047 UT, when strong HXR emission occurred, were most probably affected by the flare and are not reliable (see Fig. 5 for the position of the HXR emission relative to the longitudinal magnetic field).

There was a very rapid and substantial change in both leading and following magnetic fluxes. Immediately after the flare (at 0047 UT; Fig. 3, *right vertical dashed line*), the total leading flux increased by approximately 6%, while the total following (positive) flux decreased by about 14%. These changes were permanent, and the flux did not return back to the preflare level after the flare ended. Since we have compared total positive and negative flux measured before and after the flare, a change in the line profile during the flare is not a serious concern. Please note that the negative flux (Fig. 3, *bottom*) was continuously increasing during the observing period. We believe that this gradual growth started before the flare onset and was temporarily interrupted by the rapid fluctuations of the magnetic flux during the impulsive phase of the flare.

The apparent changes of the longitudinal magnetic field at the solar limb (Fig. 5) are artificial and purely due to the fact that variations in seeing change the position of the solar limb in the field of view between the acquisition of two consecutive circularly polarized images. When a longitudinal magnetogram is produced by subtracting one image from another, one obtains an artificial signal, which usually changes rapidly from one magnetogram to another. The noise signal at the solar limb can be distinguished from the persistent changes in an active region, which can be traced from one magnetogram to another.

We would also like to note that while the radiation measured close to the solar limb in the λ6103 photospheric spectral line is emitted from higher and thus cooler layers of the solar atmosphere, this radiation is still mainly formed in the photosphere. Thus, a contribution function for the blue wing of the Ca I λ6103 spectral line, determined close to the solar limb (Abramenko & Baranovsky 2004), shows that this part of the spectral line forms within 400 km above the τ_{5000} level, i.e., below the transition region between the photosphere and the chromosphere. Therefore, the field measurements

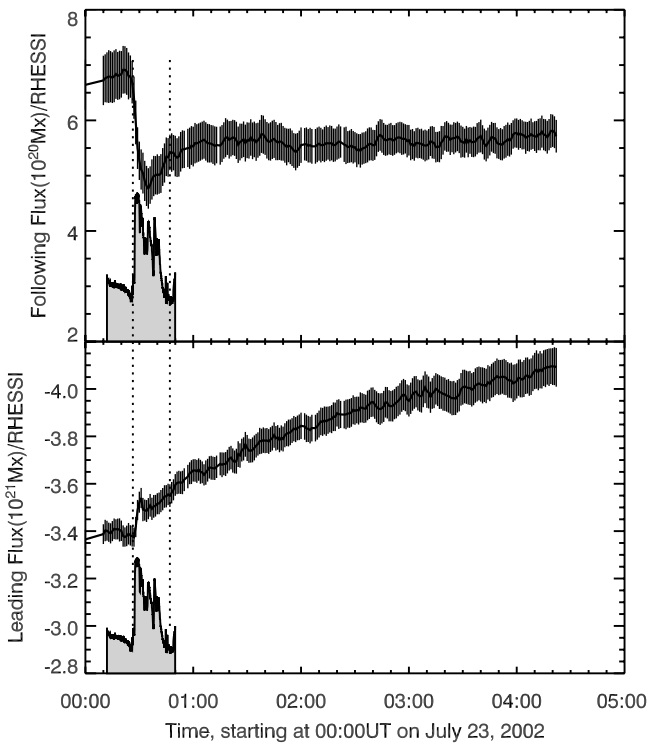

FIG. 3.—MDI positive (*top*) and negative (*bottom*) magnetic fluxes and the *RHESSI* HXR flux (*shaded area*; arbitrary units) in the 100–150 keV energy range shown as a function of time.

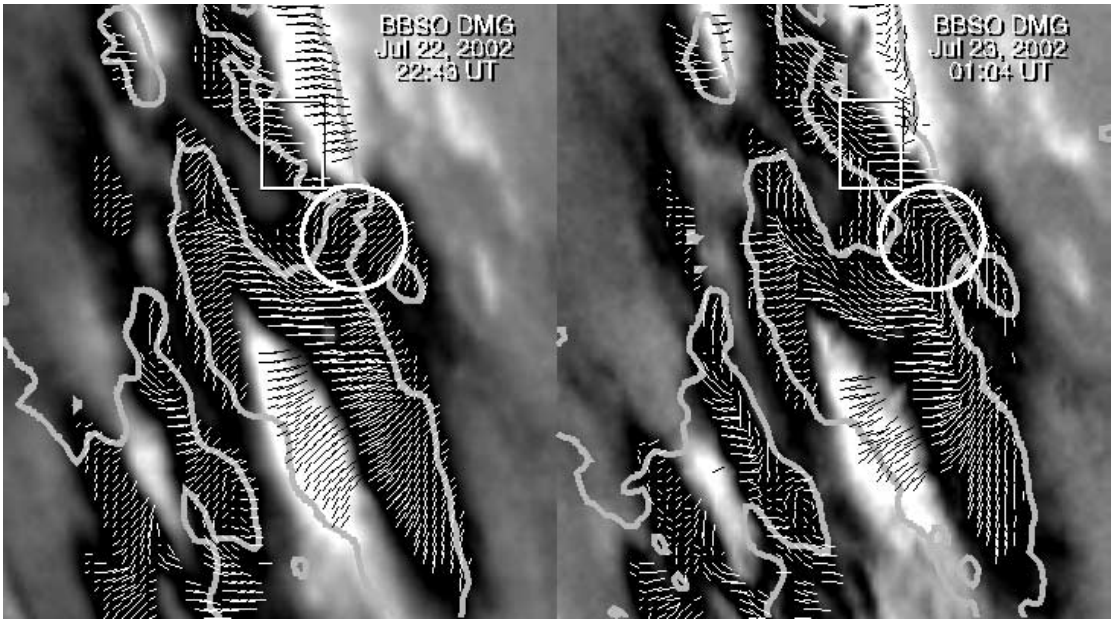

FIG. 4.—Two BBSO DMG vector magnetograms acquired before (July 22 at 2243 UT; *left*) and after (July 23 at 0104 UT; *right*) the 2002 July 23 gamma-ray flare. The backgrounds are longitudinal magnetograms (white/black correspond to ±350 G). The leading polarity is negative (black). The gray thick contours outline the photosphere-penumbra boundary of sunspots. The black and white line segments display the transverse magnetic field, while the box and circle mark the areas where the magnetic flux changes were studied in detail. North is up, and west is to the right.

made in the blue wing of the Ca I λ6103 spectral line refer to the photosphere.

Figure 4 shows two BBSO DMG vector magnetograms before (July 22 at 2243 UT) and after (July 23 at 0104 UT) the flare. Because of the close proximity of the active region to the east solar limb (the active region's longitude was $\lambda = -70^{\circ}$), we could not remove the 180° ambiguity; therefore, the line segments in Figure 4 show only the orientation of transverse magnetic fields.

We calculated the total BBSO positive and negative flux over the same area of the active region, as was done in the case of MDI data, i.e., over the entire longitudinal magnetograms shown in Figure 4. According to the BBSO data, the leading (negative) flux increased by about 5%, while the following (positive) flux decreased by about 13%. These relative changes are in very good agreement with the MDI flux variations, although the absolute values of the MDI and BBSO magnetic fluxes are somewhat different (compare the second and third columns of Table 1). This discrepancy in the absolute flux amount could be due to differences in the spatial resolution and sensitivity of the instruments.

The BBSO magnetograms in Figure 4 illustrate the changes in the longitudinal magnetic field, which we detected by calculating the total flux over the active region. The most dramatic and obvious changes occurred in two regions, marked by the circle and the box in Figures 4 and 5. The region

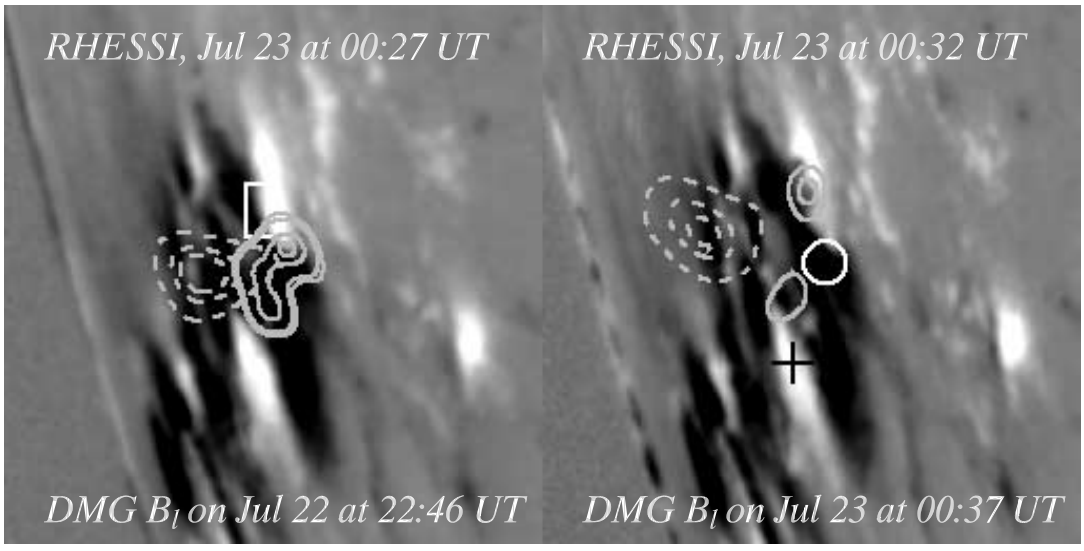

FIG. 5.—*RHESSI* data (the same as in Fig. 1) plotted over two BBSO longitudinal magnetograms (white/black correspond to ±450 G) acquired before and after the flare. The box and the circle are the same as in Fig. 4. The cross marks the position of the 2.223 MeV source centroid. North is up, and west is to the right.

TABLE 1
MAGNETIC FLUX VALUES BEFORE AND AFTER THE FLARE AS MEASURED FROM MDI AND BBSO

TIME	F^+/F^- ($\times 10^{21}$ Mx) MDI	F^+/F^- ($\times 10^{21}$ Mx) BBSO	F^- (CIRCLE) ($\times 10^{20}$ Mx)	F^- (BOX) ($\times 10^{19}$ Mx)
Before	+0.7/−3.4	+0.8/−4.2	−1.0	−1.9
After	+0.6/−3.6	+0.7/−4.4	−1.3	−5.9
Change (%)	−14/+6	−13/+5	+30	+210

marked by the circle is where the northern HXR footpoint source was located at the beginning of the flare (solid contours in Fig. 5 at 2246 UT). The magnetograms show that both the line-of-sight component and the transfer field were affected by the flare at this area: (1) the peak intensity of the longitudinal magnetic field, inside the circle, increased from −800 G to −1100 G; (2) the total negative flux increased by ∼30% from -1.0×10^{20} to -1.3×10^{20} Mx (see also the fourth column of Table 1); (3) the penumbral bridge, which connected the two major sunspots, became wider (compare the gray contours, inside the circles); (4) before the flare, the transverse field was largely oriented along the southeast-northwest line, while after the flare, the transverse field was already mainly oriented along the north-south line. All the above facts, especially the increase of the penumbral bridge, allow us to speculate that the emergence of a new magnetic flux, inside the circle, was associated with the flare. This suggestion is supported by high-resolution BBSO Hα center and off-band (−0.70 Å) images taken 2 hr before the flare peak (Fig. 6). In the center of the off-band image (*right*), one can see an elongated cold surge, indicated by the arrow, which existed for several hours before the flare. The footpoint of this surge was located inside the circle (see also Figs. 4 and 5). Also, the negative polarity (leading flux) was gradually increasing during the observed period, which may be interpreted as a signature of an emerging flux. According to Heyvaerts, Prist, & Rust (1977), the surge may indicate ongoing flux emergence in the area. Since the encircled area and the position of the earlier HXR footpoint source coincide, we can further assume that the new flux may have triggered the gamma-ray flare by alternating the topology of the magnetic field and/or adding twist to the system (Leka et al. 1996; Wang & Abramenko 2000).

Another area of great interest is marked by the box in Figure 4. The comparison of the two magnetograms shows that the negative magnetic polarity inside the box had increased threefold (from -1.9×10^{19} to -5.9×10^{19} Mx; see also the fifth column of Table 1), largely because of the devouring of the positive polarity (the position of the neutral line had shifted). The orientations of the line segments inside the box indicate that before the flare the transverse field was largely oriented along the east-west line, while after the flare it was mainly oriented along the southwest-northeast line. Distinctive from the previous case (the circled area), the increase of the penumbral area inside (and nearby) the box was not significant and could not account for the threefold increase of the negative flux. The above variations qualitatively correspond to what we would expect if the magnetic field changes its inclination by veering from the observer toward the solar limb. When the veer of the magnetic field vector becomes large enough that the angle between the line of sight and the vector of the magnetic field exceeds 90°, then the longitudinal magnetic field can change its sign, and the neutral line will shift. This seems to be the case in the event studied here. The box marks the position where the western footpoints of a rapidly evolving postflare loop (PFL) system and the northern HXR footpoint source were located in the late and gradual

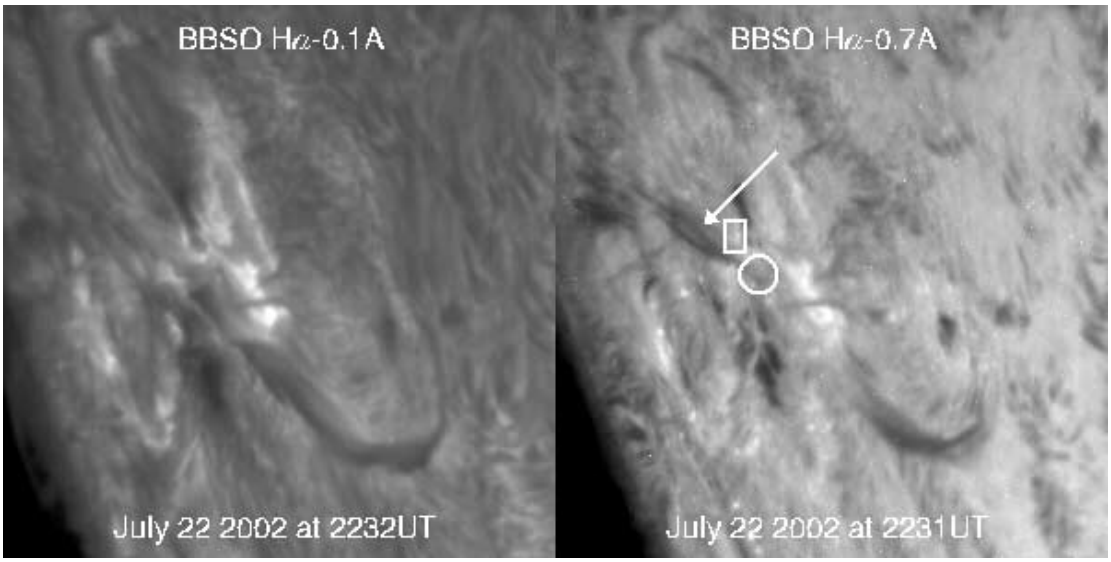

FIG. 6.—BBSO Hα center (*left*) and Hα −0.7 Å (*right*) images obtained about 2 hr before the flare. One of the footpoints of a cold surge, indicated by the arrow, is located at the position of the earlier HXR footpoint source and is probably associated with flux emergence. The box and the circle are the same as in Fig. 4. (See also Figs. 1 and 5.)

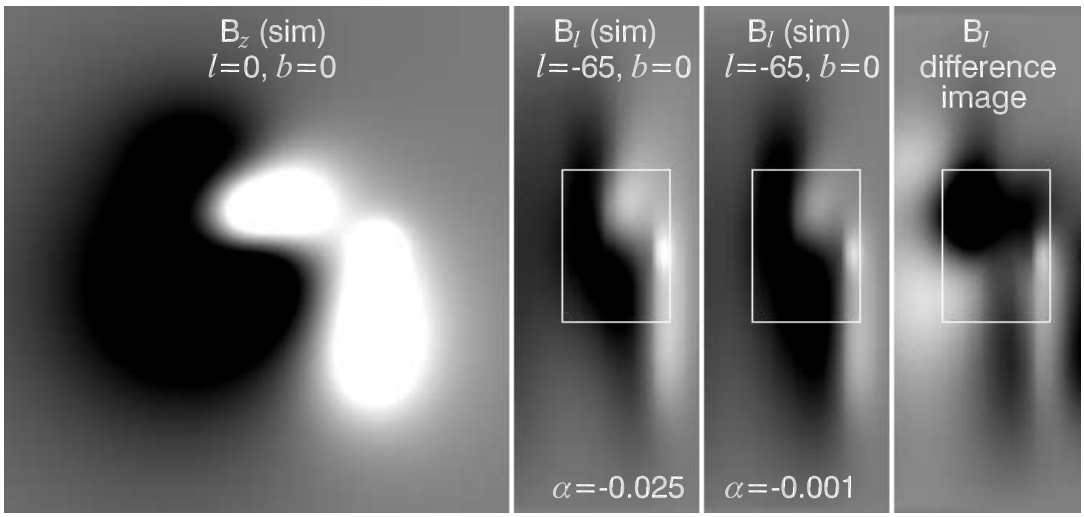

FIG. 7.—Simulated magnetograms: vertical component, B_z, shown at the center of the solar disk (*left*), and longitudinal component of an LFFF calculated with parameter $\alpha = 0.025$ arcsec^{-1} and $\alpha = 0.001$ arcsec^{-1} (*middle two panels*), as seen at the eastern solar limb. White/black is a magnetic field intensity exceeding $\pm$500 G. The right panel shows the difference image between the two longitudinal components (black represents areas where the longitudinal component decreased).

phase of the flare (see Fig. 5 at 0037 UT in the current paper and Fig. 1*f* in Krucker et al. 2003). It is known that a PFL system is a new topological link in active region, and it is expected that the magnetic field changes its orientation and/or inclination as the PFL system forms.

4.2. *Magnetic Flux Variations Inferred from the Simulated Data*

In order to find out whether the reorientation of the magnetic field is indeed capable of producing noticeable changes in the total magnetic flux, we have conducted simple simulations of a linear force-free field (LFFF). First, we constructed a B_z magnetogram with an *S*-shaped neutral line, which we used as a boundary condition (see Fig. 7, *left*). The reason for doing this was because there was no observational data for this event suitable for the modeling. Indeed, the longitudinal magnetogram, observed at $\lambda = -70^\circ$, in fact represents a component almost tangential to the solar surface, and as such it cannot be used as a boundary condition in our model.

We would like to emphasize that this numerical exercise is not meant to reconstruct the coronal magnetic field above the observed active region. This was done only to make an estimate of whether a change in the inclination of a magnetic field is capable of producing significant variations in the total magnetic flux.

In order to model a magnetic field above the simulated active region, we utilized a method to calculate an LFFF described in Abramenko & Yurchyshyn (1996). The method allows us to model a field not only by varying the force-free field parameter α, which defines the amount of twist in an active region, but also by selecting nonphotospheric boundary conditions. The upper bound of α is limited by the number of nodal points in a three-dimensional grid that we use to calculate the force-free field: the finer the grid, the smaller the α that can be used in the model. In our case we calculate an LFFF everywhere inside a $240'' \times 240'' \times 160''$ volume with a spatial resolution of $3'' \times 3'' \times 2''$.

We simulated two sets of an LFFF: one with a large amount of twist ($\alpha = -0.025$ arcsec^{-1}) and the other one with nearly potential field configuration ($\alpha = -0.001$ arcsec^{-1}). The final step in our simulations was to project modeled vector magnetograms at the eastern solar limb ($\lambda = -65^\circ$) and to calculate the corresponding line-of-sight components, which are shown in Figure 7 (*middle two panels*). The difference image between these two projected magnetograms (*right panel*) reveals that there is a significant difference between them.

The white box in Figure 7 marks the area that we used to calculate the total positive and negative magnetic flux. Our calculations indicate that in the nearly potential configuration the leading (negative) simulated flux increased by 24%, while the following (positive) polarity decreased by about 59%, as compared to the twisted configuration. Since the photospheric boundary was the same in both simulation runs (no new flux emergence), the flux variations in the simulated line-of-sight magnetograms are purely due to changes in the orientation of the magnetic field. Therefore, we conclude that the reorientation of the magnetic field is capable of producing significant variations in the observed line-of-sight magnetic flux.

5. DISCUSSION

At the beginning of this discussion we would like to summarize the observations presented in the previous sections. According to *GOES* measurements, the X4.8/2B gamma-ray flare started at 0018 UT on 2002 July 23. A noticeable gradual increase in Hα emission began at 0020 UT at the site of the flare, and no associated EUV crinkles or remote Hα emission were detected at this time. About 7 minutes later the major energy release event started, which was determined by the impulsive rise of HXR emission at 0027 UT (Fig. 2). Only after the HXR emission peaked did several remote Hα brightenings appear in a quiet-Sun region at a location about 160″north of the active region, and their intensity reached a maximum at about 0031, when the secondary peak in the HXR emission occurred. A 2218–2228 keV gamma-ray source was observed almost simultaneously with the remote Hα brightenings. However, this gamma-ray emission was located inside the active region and was displaced from the main HXR sources. The light curves of the gamma-ray source and the remote Hα brightenings were very similar during the period of their gradual increase, although the gamma-ray light

curve lagged by approximately 60 s relative to the light curve of the remote brightenings. The high time cadence MDI line-of-sight magnetograms showed that after the flare the following (positive) polarity of the active region decreased by about 14%, while the leading polarity did not show significant rapid flare-associated change: it was gradually increasing for the entire observed period. Furthermore, BBSO high-resolution vector magnetograms showed a significant increase of the penumbra area located between the Hα flare ribbons, as well as changes in the direction of the transverse magnetic field.

The multiwavelength data for the flare show that in this event, significant flare-related emission occurred in the core of the flare, prior to the occurrence of the remote Hα brightenings. The timing of this particular event does not agree with what we would expect from the breakout model, which predicts that EUV crinkles and/or remote Hα brightenings should occur prior to the major energy release event. On the other hand, the models that advocate an eruption of a preexisting flux tube (van Tend & Kuperus 1978; van Ballegooijen & Martens 1989; Forbes & Isenberg 1991; Kumar & Rust 1996; Wu et al. 1999; Amari et al. 2000) or those that require reconnection to form an unstable flux tube (Moore & LaBonte 1980) are more successful in interpreting this event because they predict that the earliest energy release event should occur in the core field at the site of a flare.

Let us now discuss, in the framework of the flux tube and tether-cutting models, one possible sequence of events during the July 23 flare. We suggest that new emerging flux, discussed in the previous section, disrupted the stability of the preexisting magnetic configuration (it may also have brought additional twist to the system) and thus triggered a large-scale eruption of the magnetic field. The erupted field stretched the field lines, which later reconnected beneath the escaping fields and formed a system of postflare loops. The footpoints of these new loops are normally seen in the chromosphere as Hα ribbons, early parts of which spatially coincide with HXR sources. As the eruption proceeds, the reconnection X-point moves upward, causing the HXR sources and Hα ribbons to move apart.

Analysis of the motion of the HXR source during the flare (see Fig. 3 of Krucker et al. 2003) showed that the coronal (Figs. 5 and 1, *dashed contours*) and the northern footpoint source (*solid contours*) were moving with comparable speeds and in similar directions, while the southern footpoint source did not display similar motions. We believe that the different motion patterns of the HXR sources is a manifestation of the upward motion of the reconnection point and was caused by different intensities of the magnetic fields at the footpoints of the PFL system. Generally speaking, during a flare equal amounts of positive and negative magnetic flux should reconnect. In the case of high-density flux (e.g., in a sunspot umbra), the footpoints of the reconnecting field lines occupy a smaller area than the low-density footpoints (say, in sunspot penumbra). Since HXR emission is a result of the precipitation of high-energy electrons at the footpoints of the reconnecting magnetic field lines, a source associated with the low-density flux will display a wider variety of displacements, while the high-density source would remain nearly stationary. Indeed, Figure 5 seems to support this explanation by showing two BBSO longitudinal magnetograms overlapped by the same *RHESSI* contours as shown in Figure 1. The stationary southern HXR footpoint was located in a strong field ($\sim$1000 G) at the umbra-penumbra border of the negative polarity sunspot, while the moving northern footpoint was associated with the much smaller positive polarity sunspot that moved along the outer edge of the sunspot penumbra, where the magnetic flux density was noticeably lower ($\sim$600 G).

We further suggest that the remote Hα brightenings and the 2218–2228 keV gamma-ray source were quite possibly caused by an interaction between the erupted field and a general large-scale magnetic field spanning the active region. After the erupted field pushed high into the corona (according to our data it was about 3 minutes after the eruption began), it may have reconnected with an overlying field. Strictly speaking, one would expect to observe Hα and X-ray signatures of this secondary reconnection both remotely and in the core region. If so, the peaks in the HXR emission detected at 0031 UT in the core of the flare and the remote Hα brightening may be signatures of this second reconnection. Note that there was no significant HXR emission detected at the remote Hα source. The X-ray counterpart of the remote Hα source was, if it existed at all, at least 25 times weaker than the main HXR sources. The increase in the Hα emission at the core site, however, could not be detected mainly because of the high Hα intensity of the core. The similarity between the light curve of the remote Hα brightenings and that of the 2218–2228 keV gamma-ray source suggests that these two sources are related and that a common process accelerated both electrons and ions. However (and against all expectations), the gamma-ray source was offset from the HXR source, and only weak Hα activity was seen in its vicinity.

Hurford et al. (2003) proposed that the offset may be a result of the acceleration that may occur far from the site of the flare. The accelerated ions traveled over a long distance before encountering the chromosphere. This explanation agrees with our suggestion of a second reconnection event high in the corona. Although the remote Hα brightenings and the gamma-ray source light curves are similar, the gamma-ray source lags the HXR emission and the remote Hα sources by about 60 s. Hurford et al. (2003) pointed out that the 2223 keV emission from deuterium is delayed by $\sim$100 s because of preceding thermalization and capturing of fast neutrons in the photosphere. The estimated and observed time delays are close, which can be interpreted as further evidence that the remote Hα source and the gamma-ray source were produced by a common acceleration process.

Finally, the question as to how and when the erupted flux tube was formed still remains open. Was an erupted flux tube formed immediately prior to the eruption, as suggested by the tether-cutting model, or was it embedded in the magnetic field long before the flare? The available data are not sufficient to make a solid conclusion. However, the observed changes in the photospheric magnetic field detected at the footpoints of the PFL system can be interpreted as being in favor of the tether-cutting model. Indeed, in the case of an eruption of a preexisting flux tube, a nearly potential overlying field stretches and recloses underneath the erupted field, thus reforming to another near-potential configuration. We therefore do not expect to see significant variations in the orientation of the field lines. However, when two (or more) sheared and independent magnetic fluxes reconnect during a flare, the sheared core field changes, so a more potential topology is reinstated, and this process should give rise to changes in the inclination and/or the orientation of the magnetic field lines, which is observed in this particular case. A two-dimensional representation of this magnetic topology is depicted in Figure 3 of Sweet (1958).

In conclusion, the tether-cutting model can successfully explain the observed occurrence of all events discussed in the

present study. We also suggest that a two-step reconnection process is required to explain the occurrence and the location of the offset gamma-ray source observed in the 2002 July 23 flare. The first reconnection occurs deep in the core field, and it is a major energy release event. The second reconnection occurs between the erupted field and a general overlying coronal field, which produces the secondary peak in HXR emission and a displaced gamma-ray source.

We are grateful to the anonymous referee for valuable comments and remarks that significantly improved the manuscript. We thank the BBSO observing staff and the *RHESSI* team for effort in obtaining the data. *SOHO* is a project of international cooperation between ESA and NASA. This work was supported in part by NSF grants ATM 02-05157 and ATM 00-86999 and NASA grants NAG5-10910 and NAG5-12782.

REFERENCES

Abramenko, V. I., & Baranovsky, E. A. 2004, Sol. Phys., in press
Abramenko, V. I., & Yurchishin, V. B. 1996, Sol. Phys., 168, 47
Abramenko, V. I., Yurchyshyn, V., Wang, H., Spirock, T. J., & Goode, P. R. 2003, ApJ, 597, 1135
Amari, T., Luciani, J. F., Mikic, Z., & Linker, J. 2000, ApJ, 529, L49
Antiochos, S. K. 1998, ApJ, 502, L181
Antiochos, S. K., DeVore, C. K., & Klimchuk, J. A. 1999, ApJ, 510, 485
Aschwanden, M. J., Fletcher, L., Schrijver, C. J., & Alexander, D. 1999, ApJ, 520, 880
Cameron, R., & Sammis, I. 1999, ApJ, 525, L61
Forbes, T. G., & Isenberg, P. A. 1991, ApJ, 373, 294
Heyvaerts, J., Priest, E. R., & Rust, D. M. 1977, ApJ, 216, 123
Hurford, G. J., Schwartz, R. A., Krucker, S., Lin, R. P., & Smith, D. M. 2003, ApJ, 595, L77
Kosovichev, A. G., & Zharkova, V. V. 1999, Sol. Phys., 190, 459
———. 2001, ApJ, 550, L105
Krucker, S., Hurford, G. J., & Lin, R. P. 2003, ApJ, 595, L103
Kumar, A., & Rust, D. M. 1996, J. Geophys. Res., 101, 15667
Leka, K. D., Canfield, R. C., McClymont, A. N., & van Driel-Gesztelyi, L. 1996, ApJ, 462, 547
Lin, R. P., et al. 2002, Sol. Phys., 210, 3
Moore, R. L., Hurford, G. J., Jones, H. P., & Kane, S. R. 1984, ApJ, 276, 379
Moore, R. L., & LaBonte, B. 1980, in IAU Symp. 91, Solar and Interplanetary Dynamics, ed. M. Dryer & E. Tandberg-Hanssen (Boston: Reidel), 207
Severny, A. B. 1964, ARA&A, 2, 363
Spirock, T. J., Yurchyshyn, V., & Wang, H. 2002, ApJ, 572, 1072
Spirock, T. J., et al. 2001, in ASP Conf. Ser. 236, Advanced Solar Polarimetry: Theory, Observation, and Instrumentation, ed. M. Sigwarth (San Francisco: ASP), 65
Sterling, A. C., & Moore, R. L. 2001, ApJ, 560, 1045
Sterling, A. C., Moore, R. L., Qiu, J., & Wang, H. 2001, ApJ, 561, 1116
Sweet, P. A. 1958, in IAU Symp. 6, Electromagnetic Phenomena in Cosmical Physics, ed. B. Lehnert (Cambridge: Cambridge Univ. Press), 123
Tang, F., & Moore, R. L. 1982, Sol. Phys., 77, 263
van Ballegooijen, A. A., & Martens, P. C. H. 1989, ApJ, 343, 971
van Driel-Gesztelyi, L., Manoharan, P. K., Pick, M., & Demoulin, P. P. 1997, Adv. Space Res., 19, 1883
van Tend, W., & Kuperus, M. 1978, Sol. Phys., 59, 115
Wang, H., Ewell, M. W., Zirin, H., & Ai, G. 1994, ApJ, 424, 436
Wang, H., Spirock, T. J., Qiu, J., Ji, H.-S., Yurchyshyn, V., Moon, Y.-J., Denker, C., & Goode, P. R. 2002, ApJ, 576, 497
Wang, H., & Tang, F. 1993, ApJ, 407, L89
Wang, T., & Abramenko, V. I. 2000, A&A, 357, 1056
Wu, S. T., & Guo, W. P. 1999, J. Geophys. Res., 104, 14,789
Yurchyshyn, V. B., Abramenko, V. I., & Carbone, V. 2000, ApJ, 538, 968
Zvereva, A. M., & Severny, A. B. 1970, Izv. Krymskoi Astrofiz. Obs., 4142, 97